Journal of Clinical Monitoring and Computing (2019) 33:269–279
https://doi.org/10.1007/s10877-018-0166-8

ORIGINAL RESEARCH

Measurement of blood-oxygen saturation using a photoacoustic technique in the rabbit hypoxemia model

Kiguna Sei[1] · Masanori Fujita[2] · Takeshi Hirasawa[3] · Shinpei Okawa[3] · Toshihiro Kushibiki[3] · Hidenori Sasa[1] · Kenichi Furuya[1] · Miya Ishihara[3]

Received: 15 June 2017 / Accepted: 31 May 2018 / Published online: 6 June 2018

Abstract
The golden standard method to obtain accurate blood oxygen saturation is blood gas analysis that needs invasive procedure of blood sampling. Photoacoustic technique enables us to measure real-time blood oxygen saturation without invasive procedure. The aim of this study is to use the photoacoustic technique, an optical method, for accurately determining oxygen saturation in vivo. We measured induced photoacoustic signals of arterial blood in the rabbit model of stable hypoxemia after irradiation at 750 and 800 nm. Oxygen saturation was calculated from the photoacoustic signals using two calibration curves. Calibration curve 1 is a conventional curve derived from the absorbance coefficient of hemoglobin, whereas calibration curve 2 is derived from the photoacoustic signals obtained from the original blood vessel model. Simultaneously, blood-gas analysis was performed to obtain the reference standard of oxygen saturation. Regression analysis and Bland–Altman analysis were performed to assess the accuracy of oxygen saturation obtained using the two methods. The oxygen saturation calculated using calibration curves 1 and 2 showed strong correlations with the reference standard in regression analysis (R = 0.965, 0.964, respectively). The Bland–Altman analysis revealed better agreement and precision with calibration curve 2, whereas there was significant underestimation of values obtained using calibration curve 1. Photoacoustic measurement of oxygen saturation using calibration curve 2 provided an accurate estimate of oxygen saturation, which was similar to that obtained using a portable blood-gas analyzer.

Keywords Photoacoustic technique · Oxygen saturation · Blood-gas analysis · Non-contact evaluation · Calibration

1 Introduction

Blood oxygen saturation is one of the most important biomedical indexes that indicates oxygenation and metabolism [1]. Although arterial blood-gas analysis is the gold standard for assessing the level of oxygenation, it requires the i nvasive method of arterial puncture for sampling blood, which may sometimes induce complications [2, 3]. Since blood sampling is required each time, arterial blood-gas analysis is not appropriate for real-time monitoring. Recently,

✉ Masanori Fujita
fujitama@ndmc.ac.jp; bxb01424@nifty.com

Kiguna Sei
sei@ndmc.ac.jp; kiguna0309@gmail.com

Takeshi Hirasawa
hirasawa@ndmc.ac.jp

Shinpei Okawa
okawa@ndmc.ac.jp

Toshihiro Kushibiki
toshi@ndmc.ac.jp

Hidenori Sasa
hsasa@ndmc.ac.jp

Kenichi Furuya
furuyakn@ndmc.ac.jp

Miya Ishihara
kobako@ndmc.ac.jp

[1] Department of Obstetrics and Gynecology, National Defense Medical College, 3-2 Namiki, Tokorozawa, Saitama 359-8513, Japan

[2] Division of Environmental Medicine, National Defense Medical College Research Institute, National Defense Medical College, 3-2 Namiki, Tokorozawa, Saitama 359-8513, Japan

[3] Department of Medical Engineering, National Defense Medical College, 3-2 Namiki, Tokorozawa, Saitama 359-8513, Japan

non-invasive methods for measuring blood oxygen saturation have been devised as alternatives to blood-gas analysis, such as pulse oximetry [4], near-infrared spectroscopy (NIRS) [5, 6], blood oxygen level-dependent magnetic imaging (BOLD-MRI) [7, 8], and photoacoustic technique.

The photoacoustic technique is one of the front-line techniques that provide real-time biological data. Photoacoustic signals, which are ultrasound waves, are generated when light-irradiated materials expand thermally [9]. Oxygen saturation can be measured by applying this technique to hemoglobin using multi-wavelength light. Photoacoustic signals from hemoglobin in blood is generated mainly from deoxyhemoglobin and oxyhemoglobin [10, 11], and the ratios of deoxyhemoglobin and oxyhemoglobin can be calculated by analyzing the photoacoustic signals.

All targets including artery, vein, and capillary vessel can be analyzed using the photoacoustic technique. Because photoacoustic signal is ultrasound wave, high spatial resolution achieved by the calculation using propagation time of photoacoustic signal is a great advantage compared to NIRS. The high spatial resolution of photoacoustic technique also enables combined imaging with B-mode ultrasound and photoacoustic image in vessels minimum diameter of 100 μm [12].

Recently, imaging of malignant tumor [13], monitoring of wound healing [14] using photoacoustic technique have been studied. However, the oxygen saturation measurement by photoacoustic technique is under development, and only few in vivo studies report the use of this method [10, 15–17] for measuring the extent of blood oxygen saturation. To the best of our knowledge, appropriate method(s) for estimating arterial blood oxygen saturation has not yet been established. The aim of this study is to establish the photoacoustic method as a low-invasive alternative for accurately measuring oxygen saturation in vivo.

We have previously reported the rabbit model of stable hypoxemia [18]. In this study, we attempted to measure blood oxygen saturation using the photoacoustic technique in this model. We used light of two different wavelengths (750 and 800 nm) to generate photoacoustic signals, and calculated oxygen saturation using two calibration curves. Simultaneously, we performed blood sampling at the same time point as the light irradiation, and measured oxygen saturation using blood-gas analysis as the reference standard.

2 Materials and methods

2.1 Definition of oxygen saturation

In this study, we selected light of two different wavelengths for irradiation, namely, 750 nm (the peak of light absorption of deoxyhemoglobin) and 800 nm (isosbestic point of deoxyhemoglobin and oxyhemoglobin) [19, 20]. We used the molar extinction coefficient of hemoglobin ε ($cm^{-1}\ M^{-1}$) published by the Oregon Medical Laser Center (OMLC) [21] (Fig. 1). We calculated the arterial blood oxygen saturation with the ratio of photoacoustic signals obtained from irradiation with either light.

In this study, oxygen saturation of hemoglobin was defined as functional oxygen saturation, where only oxyhemoglobin and deoxyhemoglobin were considered [22]. Abnormal hemoglobin such as methemoglobin or fetal hemoglobin was not considered.

We calculated oxygen saturation using the following formula (1) in this study,

$$SO_2 = \frac{[HbO_2]}{[HbO_2] + [Hb]} \times 100\ (\%). \quad (1)$$

In this formula, [Hb] represents the content volume of deoxyhemoglobin, and the $[HbO_2]$ represents the content volume of oxyhemoglobin.

We used two calibration curves for calculating the blood oxygen saturation from the photoacoustic signals and compared the accuracy of these calibration methods. One calibration curve (calibration curve 1) was derived using the molar extinction coefficient of hemoglobin, and the other calibration curve (calibration curve 2) was derived using the photoacoustic spectrum obtained from the blood vessel model that had identical diameter as that of the artery in this study.

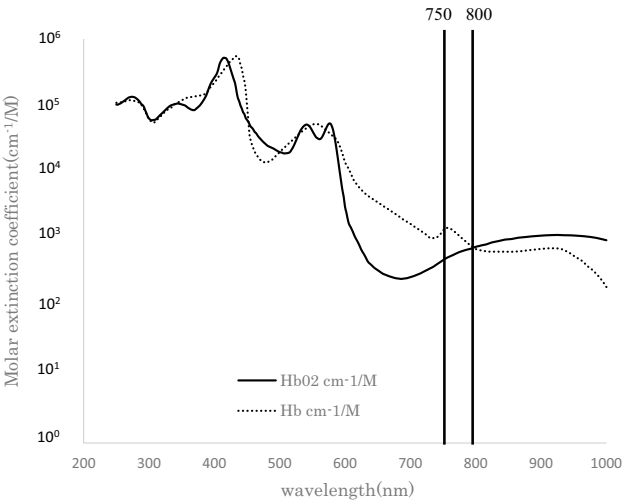

Fig. 1 Molar extinction coefficient of haemoglobin and oxidized haemoglobin. Molar extinction coefficient of haemoglobin and oxidized haemoglobin cited from the Oregon Medical Laser Center database [17]. The two vertical lines at wavelength of 750 and 800 nm were reference used in the study. The curve of haemoglobin has a peak at the wavelength of 750 nm and intersects the curve of oxidized haemoglobin at the wavelength of 800 nm

2.2 Calibration curve 1

Conventionally, the calibration method based on the molar extinction coefficient of hemoglobin published by OMLC [21] (Fig. 1) is used to calculate oxygen saturation from photoacoustic techniques or near infrared spectroscopy [11, 19, 20, 23]. We calculated the absorption coefficient μ_a of hemoglobin with certain oxygen saturation for each wavelength using the following procedure.

$$\begin{aligned}\mu_{a750} &= A_{750}[\mathrm{Hb}] + B_{750}[\mathrm{HbO_2}],\\ \mu_{a800} &= A_{800}[\mathrm{Hb}] + B_{800}[\mathrm{HbO_2}],\end{aligned} \tag{2}$$

where A_{750} and A_{800} represent μ_a of deoxyhemoglobin at 750 and 850 nm, respectively. Similarly, B_{750} and B_{800} represent μ_a of oxyhemoglobin at 750 and 850 nm. The μ_a of blood-hemoglobin at 750 and 850 nm (μ_{a750} and μ_{a800}) is expressed in the above formula. In this formula, [Hb] represents the content volume of deoxyhemoglobin and [HbO_2] represents the content volume of oxyhemoglobin.

In the published data [21] $A_{750} = 7.52\ \mathrm{cm^{-1}}$, $A_{800} = 4.08\ \mathrm{cm^{-1}}$, $B_{750} = 2.77\ \mathrm{cm^{-1}}$, and $B_{800} = 4.37\ \mathrm{cm^{-1}}$, when the hemoglobin concentration was 15 g $\mathrm{L^{-1}}$.

Since photoacoustic signal produced in the process of thermal expansion is proportional to the amount of energy absorbed from light [24], the maximum intensity of photoacoustic signal is proportional to μ_a.

The maximum intensity of photoacoustic signals, p, [volt $\mathrm{Joule^{-1}}$ (V $\mathrm{J^{-1}}$)] is expressed in formula (3) [25]. The K in formula (3) is a value determined by the material-specific constant (Grueneisen constant) and the intensity of light reaching the material,

$$p = K\mu_a. \tag{3}$$

The maximum intensity of photoacoustic signal generated using light of wavelengths 750 and 850 nm are represented as p_{750} and p_{800} and were calculated using the following formula,

$$\begin{aligned}p_{750} &= 7.52 \times K[\mathrm{Hb}] + 2.77 \times K[\mathrm{HbO_2}],\\ p_{800} &= 4.08 \times K[\mathrm{Hb}] + 4.37 \times K[\mathrm{HbO_2}].\end{aligned} \tag{4}$$

In this formula, [Hb] represents the content volume of deoxyhemoglobin and [HbO_2] represents the content volume of oxyhemoglobin.

Oxygen saturation (Sc_1O_2) was calculated using the following equation.

$$\begin{aligned}Sc_1O_2 &= \frac{A_{750}p_{800} - A_{800}p_{750}}{(B_{800} - A_{800})p_{750} - (B_{750} - A_{750})p_{800}}\\ &= \frac{7.52 \times p_{800} - 4.08 \times p_{750}}{0.29 \times p_{750} + 4.75 \times p_{800}}.\end{aligned} \tag{5}$$

Figure 2 shows calibration curve 1. The x-axis shows the oxygen saturation and the y-axis shows the ratio of p_{750} and p_{800},

$$\frac{p_{750}}{p_{800}} = \frac{7.52 \times [\mathrm{Hb}] + 2.77 \times [\mathrm{HbO_2}]}{4.08 \times [\mathrm{Hb}] + 4.37 \times [\mathrm{HbO_2}]}. \tag{6}$$

We obtained photoacoustic signals from rabbit arterial blood, and Sc_1O_2 was calculated using these signals and calibration curve 1.

2.3 Calibration curve 2

Blood (14.7 mL) was sampled from the auricular vein of a healthy male rabbit (3 kg body weight). This volume was less than 15% of the total blood volume and did not affect the physiological state [26]. Heparin sodium (300 IU; 0.3 mL) was added to prevent coagulation, and the final concentration of heparin was adjusted to 20 IU $\mathrm{mL^{-1}}$ [27].

We set up a blood vessel model with a water tank (10 cm width, 10 cm depth, and 5 cm height) and three French polyvinyl chloride tubes (external diameter: 1 mm, internal diameter: 0.7 mm, Atom Indwelling Feeding Tube for Infant, 43003, Atom Medical Co. Saitama, Japan), and heparinized blood with 0 and 100% oxygen saturation was sealed in the tube (Fig. 3).

Blood with 0% oxygen saturation was prepared by adding 5 mg sodium dithionite ($Na_2S_2O_4$) to 1 mL blood [28].

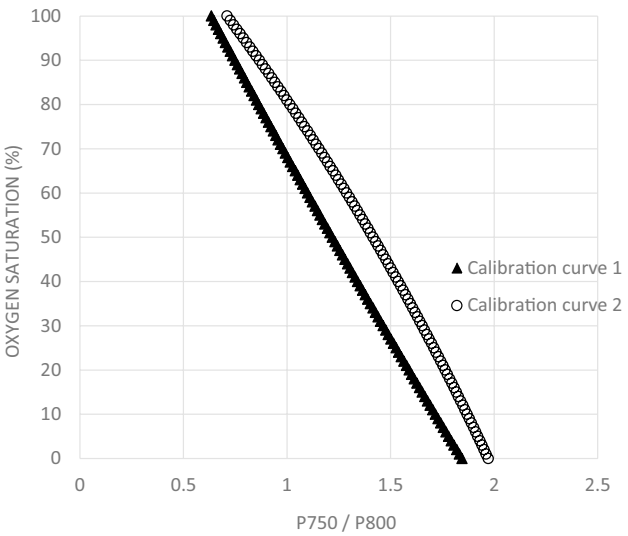

Fig. 2 Calibration curves obtained from absorption coefficient of hemoglobin and our study. Figure shows calibration curve 1 and 2. The oxygen saturation can be calculated from the ratio of intensity of photoacoustic signals by 750 and 800 nm lights. Calibration curve 1 is based on molar extinction of absorption of hemoglobin and oxidized hemoglobin [17] (Fig. 1). Calibration curve 2 is based on the photoacoustic signals obtained from the blood vessel model in Fig. 3

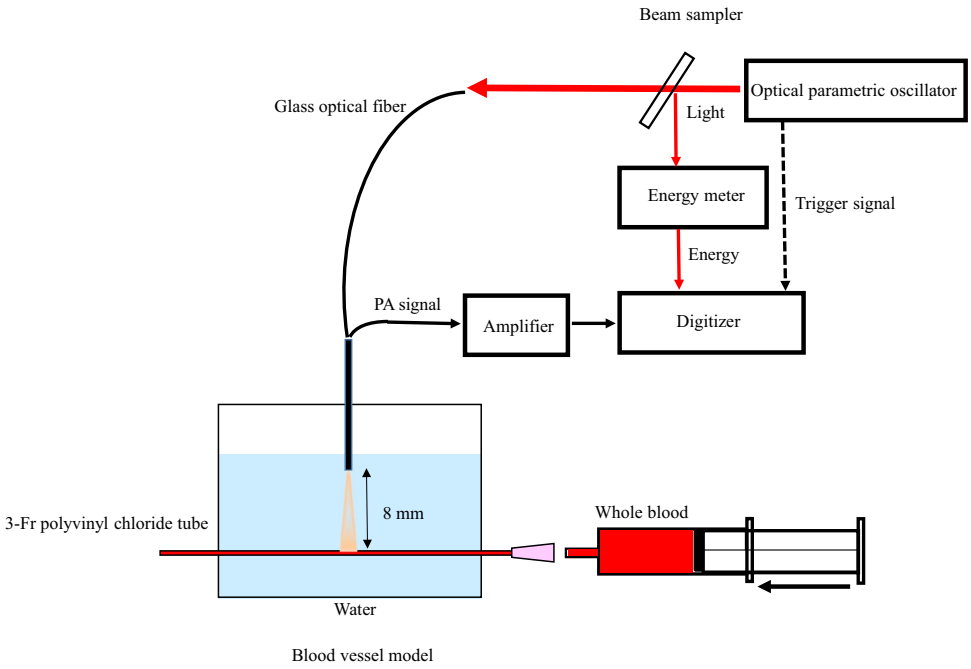

Fig. 3 Experimental setup for photoacoustic measurement of blood vessel model. Blood vessel model was build up with a water tank and a 3-Fr polyvinyl chloride tube. Heparinized whole rabbit blood was injected in the tube and photoacoustic signal with lights of 750 and 800 nm was obtained right after the injection. The blood with 0% oxygen saturation was presented by rabbit blood added sodium dithionite ($Na_2S_2O_4$). The blood with 100% oxygen saturation was presented by rabbit blood bubbled by 100% oxygen for 2 min. The focal distance of the photoacoustic probe was 8 mm. The strength of light was monitored by the energy meter. The same photoacoustic instruments was used in the measurement in vivo (Fig. 4)

Blood with 100% oxygen saturation was prepared by bubbling oxygen for 2 min in blood according to an established method [17]. We confirmed the extent of oxygen saturation of blood sealed in the blood vessel model using a portable blood-gas analyzer (i-STAT; Abbott Point of Care Inc., Princeton, NJ, USA) with a cartridge (CG4+; Abbott Point of Care Inc., Princeton, NJ, USA).

The maximum intensities of photoacoustic signals from the blood vessel model with 0 and 100% oxygen saturation were obtained, which were represented in the following formula,

$$\begin{aligned} p_{750} &= \mathrm{P}^{0}_{750}[\mathrm{Hb}] + \mathrm{P}^{100}_{750}[\mathrm{HbO_2}], \\ p_{800} &= \mathrm{P}^{0}_{800}[\mathrm{Hb}] + \mathrm{P}^{100}_{800}[\mathrm{HbO_2}], \end{aligned} \tag{7}$$

where P^{0}_{750} and P^{0}_{800} represent the maximum intensities of 0% oxygen-saturated sample at 750 and 850 nm, respectively. P^{100}_{750} and P^{100}_{800} present the maximum intensities of 100% oxygen-saturated sample at 750 and 850 nm.

In this formula, [Hb] represents the content volume of deoxyhemoglobin and [HbO_2] represents the content volume of oxyhemoglobin.

The results obtained from the blood vessel model are followings: $\mathrm{P}^{0}_{750} = 1220\ \mathrm{V\ J^{-1}}$, $\mathrm{P}^{0}_{800} = 618\ \mathrm{V\ J^{-1}}$, $\mathrm{P}^{100}_{750} = 346\ \mathrm{V\ J^{-1}}$, and $\mathrm{P}^{100}_{800} = 488\ \mathrm{V\ J^{-1}}$.

Thus, similar to Sc_1O_2, the oxygen saturation (Sc_2O_2) calculated from photoacoustic intensity using the calibration curve 2 is presented in formula (8).

$$\begin{aligned} \mathrm{Sc_2O_2} &= \frac{\mathrm{P}^{0}_{750}p_{800} - \mathrm{P}^{0}_{800}p_{750}}{(\mathrm{P}^{100}_{800} - \mathrm{P}^{0}_{800})p_{750} - (\mathrm{P}^{100}_{750} - \mathrm{P}^{0}_{750})p_{800}} \\ &= \frac{1220 \times p_{800} - 618 \times p_{750}}{874 \times p_{800} - 130 \times p_{750}}. \end{aligned} \tag{8}$$

Calibration curve 2 shown in Fig. 2 was plotted with the oxygen saturation on the x-axis, and the ratio of p_{750} and p_{800} calculated from formula (6) on the y-axis,

$$\frac{p_{750}}{p_{800}} = \frac{1220 \times [\mathrm{Hb}] + 346 \times [\mathrm{HbO_2}]}{618 \times [\mathrm{Hb}] + 488 \times [\mathrm{HbO_2}]}. \tag{9}$$

We converted the maximum intensities of photoacoustic signal to oxygen saturation (Sc_2O_2), using calibration curve 2.

2.4 Photoacoustic instrumentation

The experimental setup of the blood vessel model for photoacoustic measurement is shown in Fig. 3. As the excitation light, pulsed light was generated by tunable optical parametric oscillator pumped by third harmonic generation of Nd YAG laser (Versascan MBI-FE, Spectra-Physics, Inc. Santa Clara, CA, USA). The duration of the pulse was 6–8 ns and the repetition frequency was 10 Hz. The change in light energy was observed using an energy meter (PE25-C, Ophir Optics, Jerusalem, Israel).

The photoacoustic probe used consisted of a 600 µm-wide optical glass fiber surrounded by a focused acoustic sensor [29]. The acoustic sensor was made from a co-polymer film of polyvinylidene fluoride-ethylene trifluoride (PVDF-TrFE). The focal distance, external diameter, and internal diameter were 8, 5.0, and 1.4 mm, respectively. The sensitivity of the sensors in bandwidth of 0.5–17.4 MHz was − 6 dB. The photoacoustic signals detected by the acoustic sensors were amplified by a low noise amplifier (SA-220F5, NF Electronic Instruments, Corp., Yokohama, Japan), and recorded using a 10-bit digitizer (M9210A, Agilent Technologies, Santa Clara, CA, USA) with 100 MSa s^{-1} (mega samples per second) sampling rate.

2.5 In vivo measurement of oxygen saturation

2.5.1 Animal preparation

We used rabbits older than 4–6 month in the experiment because they are considered as adults in the literature [30]. Seven adult female Japanese white rabbits were purchased from Kitayama Labs Co., Ltd. (Nagano, Japan). The health of the animals was checked at the time of installation, and each animal was maintained in separate units in the animal rearing facility for more than one week before the experiments to acclimatize them to the environment. Animals were given ad libitum access to pellet and water. Room temperature of 25 ± 1 °C and 50 ± 5% humidity were maintained with 12 h of light–dark cycle.

Experimental preparation, including shaving, sedation, disinfection, surgical preparation, and monitoring were performed using the same procedure as previously reported [18]. The rabbits were sedated by injecting a mixture of 35 mg kg^{-1} ketamine (Sankyo, Tokyo, Japan) and 5 mg kg^{-1} xylazine (Nihon Zenyaku Kogyo, Fukushima, Japan) into the gluteal muscle per conventional methods [31]. The rabbits were covered with heating blankets (Homeothemic Monitor K020917, Harvard Apparatus, MA, USA) throughout the experiment, and rectal temperature was measured. The rectal temperature of rabbits ranged from 39.02 to 40.13 °C [32] throughout the experiment. All surgical procedure was performed under sterile conditions. A 23-gauge catheter (Surflo, Terumo, Tokyo, Japan) was inserted in the left auricular vein and 6 mL kg^{-1} h^{-1} [33, 34] physiological saline (Otsuka Seiyaku, Tokushima, Japan) was infused.

The median incision in the cervical area and intubation by tracheotomy were performed. The rabbits were ventilated with room air at initial respiratory rate of 40 min^{-1} and tidal volume of 20.0 mL using a ventilator (Volume Control 155–7058, Harvard Apparatus, MA, USA), which was calculated as the normal physiological value for 3.0 kg body-weight of rabbits using an established formula [35, 36]. Figure 4 shows the experimental setup.

General anesthesia was maintained using 1.0% sevoflurane [37] (Maruishi Pharmaceutical, Osaka, Japan) inhalation and intravenous infusion of 0.6 mg kg^{-1} rocuronium bromide. Additional 0.6 mg kg^{-1} rocuronium bromide was infused when spontaneous movement or respiration were observed [34]. More than 40 mmHg of mean arterial pressure (or systolic pressure above 60 mmHg) was maintained to retain cerebral perfusion by controlling the concentration of sevoflurane from 0.5 to 2.0% [37–39].

The caudal end of the cervical median incision was extended to the right, and the proximal portion of the right subclavian artery was exposed. A 22-gauge catheter (Surflo® ETFE, Terumo, Tokyo, Japan) was inserted through carotid artery with the top of the catheter placed at the crossing point of the carotid and subclavian arteries. The lumen of the catheter and line were filled with saline with 125 units of heparin per 500 mL saline to avoid coagulation, and direct measurement of arterial blood pressure was started [40].

We conformed to the anatomical name of the vessels reported by Zotti [41].

2.6 In vivo photoacoustic measurement

The respiration rates of the rabbits were changed in five stages, from 40 to 30, 20, 30, and 40 min^{-1}, according to the procedure described in our previous study [18]. We previously showed that the oxygen saturation was stable from 0.5 to 20 min after changing the respiratory rate [18], and we performed the photoacoustic measurement during this period.

The light was irradiated on the crossing point of the carotid and subclavian arteries such that the light did not irradiate the catheter itself but was close to the tip of catheter (Fig. 4). The time required for photoacoustic measurement was 2 s per wavelength. Blood was sampled via the catheter and the oxygen saturation was measured using i-STAT as the reference (SaO_2) prior to the photoacoustic measurement. We performed one set of measurement of blood sample and photoacoustic signals for each respiratory rate, and a total of five sets of measurements were made for each rabbit. We obtained 35 time points of measurements in seven rabbits.

2.7 Assessment of oxygen saturation using the photoacoustic technique and statistical analysis

Twenty-one photoacoustic signals of each wavelength were obtained from one measurement because the observation time was 2 s and the pulse frequency was 10 Hz. We calculated the average of the intensities of the 21 signals to obtain p_{750} and p_{800}. We applied p_{750} and p_{800} to calibration curves 1 and 2 to obtain Sc_1O_2 and Sc_2O_2, respectively.

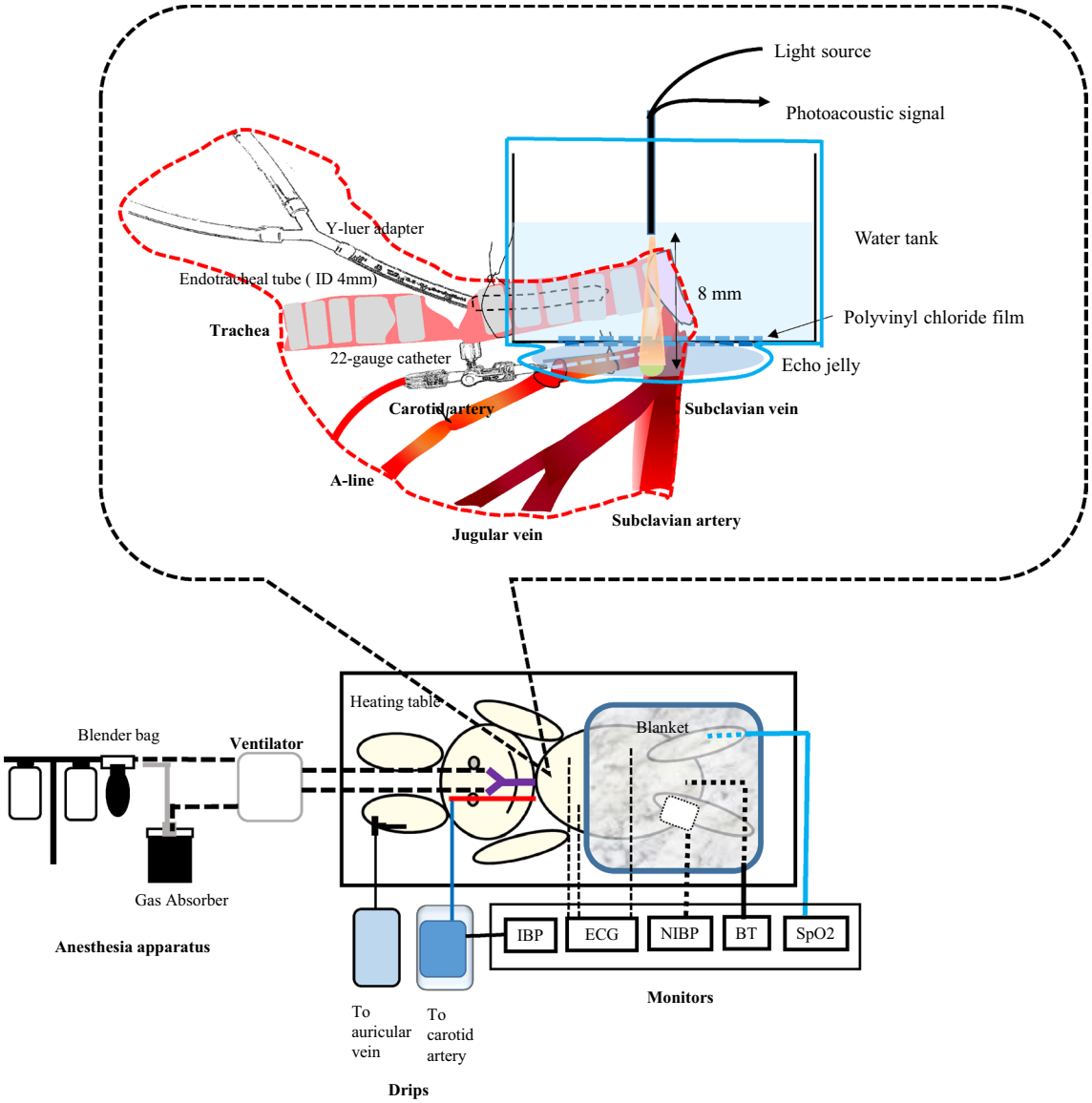

Fig. 4 Experimental setup for measurement in vivo. The figures show the experimental instruments setup. *IBP* invasive blood pressure, *IBP* invasive blood pressure, *ECG* electrocardiograph, *NIBP* noninvasive blood pressure, *BT* body temperature, SpO_2 arterial oxygen saturation measured by pulse oximetry. Surgical field (area encircled by red broken line). Intubation was performed with a endotracheal tube (ID 4 mm) cut to 11 cm length. The tube was connected to the ventilator through a bifurcated Y-luer adapter and silicon tubes (ID 4 mm). The distal side of carotid artery is ligated. Cannulation into carotid artery is performed using 22-gauge catheter with cut down procedure. The tip of the catheter is placed at the origin of the carotid artery and catheter is ligated with artery. The subclavian artery was exposed. The yellow round on the origin of subclavian artery presents the point of light radiation to measurement of photoacoustic signal. Setups for photoacoustic measurements (area encircled by blue line). Photoacoustic measurements were performed by the same instrument setup shown in Fig. 3. The bottom of the tank was removed and the hole was covered by clear polyvinyl chloride film. The lights of 750 and 800 nm wavelength were radiated through the tank filled up with water. Echo jelly was filled between the tank and the exposed artery

We used two statistical analysis methods to assess the accuracy of Sc_1O_2 or Sc_2O_2. SaO_2 is reference data obtained using the blood-gas analyzer. Initially, linear regression analysis was performed to assess the correlation between SaO_2 and Sc_1O_2 or Sc_2O_2. Secondly, the Bland–Altman analysis was performed for evaluating the details of the two calibration methods. Agreement and precision were assessed by the bias and width of 95% limits of agreement (95% LOA) [42, 43]. In the student-t test, we used t value = 2.03 when degree of freedom was 34, and confidential interval was 95%.

Statistical analysis was performed using the statistical software JMP® Pro version 11.2.0 (SAS Institute Ltd., Cary, NC, USA).

3 Result

We obtained 35 points of data (5 points per rabbit) from 7 female adult rabbits (body-weight 3.10 ± 0.09 kg; mean ± standard deviation). The maximum fluence of irradiated light was 3.18 mJ cm^{-2}, and 100–200 μJ per pulse. The energy of the light was within the safety range of laser irradiation to the human body established by the American National Standard for Safe Use of Lasers Z136.1 [44].

We performed all photoacoustic measurements and blood sampling from 0.5 to 20 min after changing the respiratory rate since our previous study demonstrated that arterial blood oxygen saturation was stably maintained in this period [18]. The results of arterial blood gas analysis were shown in Table 1.

The scatter plots of Sc_1O_2 and SaO_2, and Sc_2O_2 and SaO_2, and the results of linear regression analysis are shown in Fig. 5. The obtained regression formulae of Sc_2O_2 and S_1O_2 are shown below.

$$\begin{aligned} Sc_1O_2 &= 1.44 \times SaO_2 - 50.2 \ (p < 0.001), \\ Sc_2O_2 &= 1.13 \times SaO_2 - 11.5 \ (p < 0.001). \end{aligned} \quad (10)$$

The correlation coefficient R of Sc_1O_2 and Sc_2O_2 were 0.965 and 0.964, respectively. The standard error of Sc_1O_2 and Sc_2O_2 were 3.18 and 2.51, respectively.

The Bland–Altman plot is shown in Fig. 6. We computed the 95% LOA of Sc_1O_2 with the upper limit as − 8.38 (95% confidential interval CI; − 25.6 to 8.84) and the lower limit as − 11.5 (95% CI; − 28.7 to 5.72). This negatively deviating 95% LOA revealed that Sc_1O_2 had negative fixed biases. This result indicated that the calibration method of calibration curve 1 always underestimated oxygen saturation. The 95% LOA of Sc_2O_2 with the upper limit as 0.675 (95% CI;

Table 1 The result of arterial blood gas analysis of the seven rabbits in each step

Respiration rate (min^{-1})	SaO_2 (%)	pH	$PaCO_2$ (mmHg)	PaO_2 (mmHg)
40	97.7 ± 0.7	7.45 ± 0.09	23.9 ± 4.4	93.2 ± 11.6
30	89.0 ± 5.7	7.28 ± 0.10	33.5 ± 5.8	67.8 ± 14.0
20	77.6 ± 2.7	7.24 ± 0.09	41.4 ± 5.6	49.6 ± 4.1
30	84.6 ± 3.8	7.27 ± 0.09	35.1 ± 7.1	57.2 ± 8.0
40	95.8 ± 1.3	7.33 ± 0.06	27.0 ± 4.6	86.6 ± 10.6

(Average ± SD)

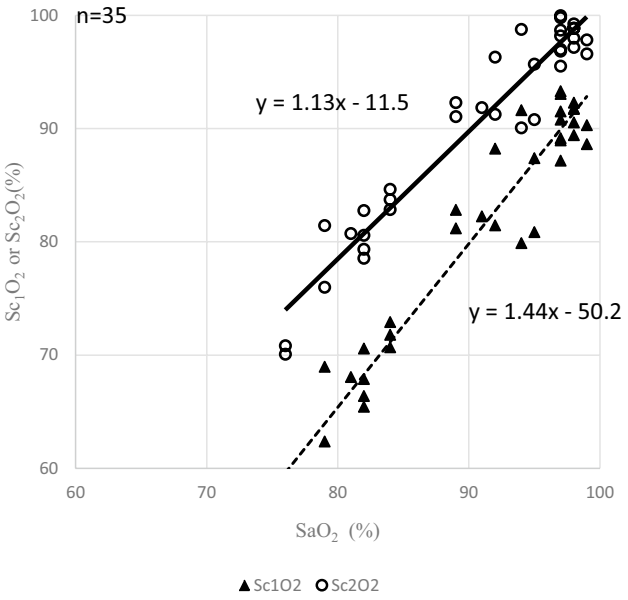

Fig. 5 Results of linear regression analysis of SaO_2 and Sc_1O_2 or Sc_2O_2. Solid triangles shows correlation between Sc_1O_2 and SaO_2 and the regression line is presented by broken line. Open circles shows correlation between Sc_2O_2 and SaO_2 and the regression line is presented by solid line. The correlation coefficient R of Sc_1O_2 and Sc_2O_2 were 0.965 and 0.964, respectively. The standard error of Sc_1O_2 and Sc_2O_2 were 3.18 and 2.51, respectively

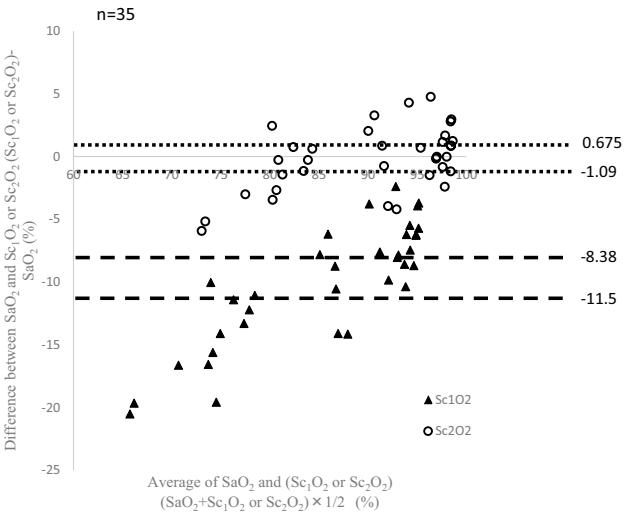

Fig. 6 Bland–Altman plotting and 95% limits of agreement. The broken lines present the upper and the lower limits of 95 % limits of agreement (LOA). The broken lines; Sc_1O_2 (− 11.5 to − 8.38), the dotted lines; Sc_2O_2 (− 1.09–0.675). Solid triangles shows the value of Sc_1O_2. Sc_1O_2 has negative error in almost all spots and the underestimation increased in lower oxygen saturation level. Open circles shows the value of Sc_2O_2. Sc_2O_2 had no fixed bias and no proportional bias. The width of LOA in Sc_2O_2 was significantly less than in Sc_1O_2

0.319–1.03) and the lower limit as − 1.09 (95% CI; − 1.44 to − 0.731) indicated no fixed biases.

The t-value of Sc_1O_2 was 13.0, which was larger than t = 2.03. This result showed that negative proportional biases were present in Sc_1O_2, and that the underestimation of oxygen saturation in Sc_1O_2 increased at lower oxygen saturation levels. The t-value was 0.475 and there was no proportional bias in Sc_2O_2. The width of 95% LOA of Sc_1O_2 and Sc_2O_2 were 3.12 and 1.76, respectively, which showed that Sc_2O_2 exhibited higher precision than Sc_1O_2.

4 Discussion

We obtained photoacoustic signals from arterial blood using the rabbit model of stable hypoxemia and arterial blood samples that were collected in parallel with the photoacoustic measurements. Thirty-five sets of photoacoustic signals and blood-gas analysis were obtained from seven rabbits. Oxygen saturation was calculated using the photoacoustic signals applied on two calibration curves and by blood-gas analysis. We compared the two values of oxygen saturation (Sc_1O_2 and Sc_2O_2) calculated using calibration curves 1 and 2 with that measured using blood-gas analysis (SaO_2). The correlation, agreement, and precision among these measurements were statistically analyzed.

Close correlation between Sc_1O_2 and SaO_2 (R = 0.965), and Sc_2O_2 and SaO_2 (R = 0.964) were detected using the linear regression analysis. However, the standard error was higher for Sc_1O_2 than for Sc_2O_2 (3.18 and 2.51, respectively), which indicated that there was larger dispersion from the regression line for Sc_1O_2 than for Sc_2O_2. The Bland–Altman analysis was performed for detailed assessment. The analysis revealed higher agreement between Sc_2O_2 and SaO_2 than between Sc_1O_2 and SaO_2. Sc_1O_2 showed fixed and significant proportional biases. Further, calibration curve 1 underestimated oxygen saturation and the error increased in lower range of oxygen saturation. Compared to SC_1O_2, the values obtained with Sc_2O_2 were closer to those obtained with SaO_2.

Calibration curve 1 is based on the conventional method that is widely used in the field of photoacoustic imaging to visualize hypoxic areas [23, 45, 46]. However, this method considers only absorption of light and neglects the effect of light scattering [10, 47]. The light propagation pathway in blood is assumed straight in this method. Nonetheless, light is both absorbed and scattered when it propagates in blood, and several studies reported that light scattering should be considered for absolute measurement of blood oxygen saturation [48]. The red blood cell possesses a disc-shaped and concave morphology. In red blood cells, 34 g dL^{-1} hemoglobin is enclosed by a 7 nm-thick lipid bilayer membrane [49]. Light does not transmit straight in red blood cells, and refraction at the cell wall results in a complicated optical propagation [50]. This renders the optical path length longer in blood than in a hemoglobin solution where light propagates straightly.

The Lambert–Beer's law determines the light intensity (ΔI) absorbed by materials as follows.

$$\Delta I = I_0 - I = I_0\left(1 - \exp\left(-\mu_a d\right)\right). \tag{11}$$

In this formula, I_0 is the intensity of irradiated light, I is the transmitted light intensity, μ_a is absorption coefficient, and d is the optical path length. As shown in formula (3), the intensity of photoacoustic signal depends on the energy of light absorbed by the material. Therefore, ΔI determines the intensity of photoacoustic signals. According to the modified Lambert–Beer's law, loss of light in the scattering medium depends on the total path length [51]. Since the optical path length (d) increases in scattering medium, ΔI and K in formula (3) increase and p is enhanced. Friebel et al. studied the absorption of washed red blood cell liquid by the integrating sphere technique. They reported that light absorption of the red blood cell liquid was approximately twice as strong as a hemoglobin solution with identical hemoglobin concentration [52] Light scattering in red blood cells would, therefore, increase absorption.

In the calculation of oxygen saturation using calibration curve 1, [Hb] and [HbO_2] can be overestimated because the enhancement of the intensity of photoacoustic signals was attributed to the increase of [Hb] and [HbO_2]. However, this increase actually depends on the increase in d. In the method using calibration curve 2, the error due to scattering is corrected because the reference photoacoustic signals in calibration curve 2 were obtained from blood. Although, the relationship between strength of scattering and the optical path length in the real blood vessel of rabbits is unclear, the overestimation of [Hb] and [HbO_2] can cause the underestimation of oxygen saturation when calibration curve 1 is used. According to formula (1), the overestimation of [Hb] would be the main cause of the negative error of Sc_1O_2.

We considered the effect of only normal functional hemoglobin and excluded the possible effects of abnormal hemoglobin, including methemoglobin, monocarboxyhemoglobin, and fetal hemoglobin because of their limited presence in the healthy body. Abnormal hemoglobin in healthy human body is less than 1.5% and contributes negligibly to the measurement of oxygen saturation in general condition [53].

This study had two limitations. One was the range of oxygen saturation, which is 70–100%. This range limitation was due to the capacity of the blood gas analyzer and restriction of measurement object, i.e., artery only. Because the performance limit of the blood-gas analyzer (i-STAT®) in this experimental setup is considered reproducible and

accurate in oxygen saturation range higher than 70% [54, 55], we had to limit the range of oxygen saturation within relatively narrow, and high range. The standard for oxygen saturation measurement defined by International Organization for Standardization (ISO) is a CO oximeter.

Although lower range of blood oxygen saturation could be measured by venous blood, our previous study showed the instability of venous blood gas. Moreover, some studies reported that venous blood oxygen saturation differed two points with only 5-mm distance [56]. We did not measured venous blood for these results because our aim was precise validation of oxygen saturation. However, our results in relatively low oxygen saturation range (around 70%) demonstrated close to the values by blood gas analysis. The method of calibration curve 2 would be applied well enough in the range below 70%.

Second limitation is deficiency of no-invasiveness. In this study, surgical exposure of artery was performed to omit the influence by skin layer. In "no-invasive" measurement method, transcutaneous measurement procedure should be established. In transcutaneous measurement, the confirmation of vessel location is essential. Although a combined system of B-mode ultrasound and photoacoustic imaging is ideal for transcutaneous measurement, the system has not been developed. The strongest advantage of photoacoustic technique is that photoacoustic technique is a method to measure ultrasound waves and this means that a construction of the combined system is possible. We already developed the system with one wavelength irradiation light [12]. The development of the system with multiple wavelength lights is our future work.

Due to high spatial resolution, photoacoustic technique is advantageous than other non-invasive bed-side technique such as pulse oximeter and NIRS. Although pulse oximeter is the most widely-used equipment to measure arterial blood oxygen saturation, its object is limited to peripheral artery. NIRS is now spreading in clinical monitoring to measure the change of oxygen saturation in tissues. However, NIRS, which observes attenuation of irradiated light in tissues, the spatial resolution is much lower than photoacoustic technique because the light propagation pathway is unclear due to scattering. The value measured by NIRS is similar to average blood oxygen saturation of all the tissues where the irradiated light propagates, and the measurement of blood oxygen saturation of a specific vessel or a region of interest is extremely difficult by NIRS. Moreover, it was reported that the change of hemoglobin volume in tissues such as ischemia or anemia would influence on the NIRS data [57]. In the photoacoustic technique, the oxygen saturation is calculated as the ratio of two photoacoustic signal intensities that correlate to [Hb] and [HbO_2], and total hemoglobin concentration was offset in calculation. Thus, oxygen saturation measurement by photoacoustic technique is not affected by hemoglobin volume. This is an advantage of photoacoustic technique that can measure blood oxygen saturation without being influenced by change of hemoglobin volume might expand the usability of intraoperative monitoring of vessels. Monitoring of feeding vessels of specific organs such as liver, lung, and intestinal canal, where blood sampling cause massive hemorrhage, might yield surgical procedure. Surface vessels of placenta and umbilical vessels that are exposed in fetoscopy would be included in the objects.

Photoacoustic technique is expected as a new technique for clinical monitoring. Ultrasound imaging combined with real-time measurement of oxygen saturation will improve the ultrasound examination. Consideration of both absorbance and scattering may be necessary for accurately calculating oxygen saturation from photoacoustic signals.

5 Conclusion

We performed in vivo photoacoustic signal measurement of rabbit arterial blood and blood samples collected using the invasive sampling method. Blood-oxygen saturation was computed from 35 sets of photoacoustic signals and blood-gas analyzer measurements. We used two types of calibration methods for determining oxygen saturation from the photoacoustic signals, namely, the conventional method (calibration curve 1) and the original blood vessel-based model (calibration curve 2). Statistical analysis showed that calibration curve 2 computed oxygen saturation accurately, which were similar to the results obtained using, i-STAT, a portable blood gas analyzer. Calibration curve 1 analyzed only light absorption, and therefore, calculated lower values than those obtained with blood-gas analysis, which resulted in underestimation of the oxygen saturation level. This result indicated that a calibration method that considers both absorption and scattering of light was required for accurate photoacoustic measurement of blood oxygen saturation.

Acknowledgements We would like to express our gratitude to the support by National Defense Medical College Animal Experiment Facility and Mr. Yuta Ikeda for his dedicated assistance to collect data. This study was partly supported by Japan Society for the Promotion of Science (KAKENHI, Grant Number 16K16413).

Funding This study was supported by the fund of National Defense Medical College and Japan Society for the Promotion of Science (KAKENHI, Grant Number 16K16413).

Compliance with ethical standards

Conflict of interest All authors declare that they have no conflict of interest to disclose.

Ethical approval The experimental protocol used in this study was approved by the Institutional Review Board on Animal Care of National Defense Medical College, Japan (Approval number; 13091).

References

1. Toffaletti J, Zijlstra WG. Misconceptions in reporting oxygen saturation. Anesth Analg. 2007;105(6):S5–9.
2. Scheer BV, Perel A, Pfeiffer UJ. Clinical review: complications and risk factors of peripheral arterial catheters used for haemodynamic monitoring in anaesthesia and intensive care medicine. Crit Care. 2002;6(3):1.
3. O'grady NP, Alexander M, Burns LA, Dellinger EP, Garland J, Heard SO, et al. Guidelines for the prevention of intravascular catheter-related infections. Am J Infect Control. 2011;39(4):S1-34.
4. Severinghaus JW. Takuo Aoyagi: discovery of pulse oximetry. Anesth Analg. 2007;105(6):S1–4.
5. Hasegawa J, Nakamura M, Matsuoka R, Mimura T, Ichizuka K, Sekizawa A, et al. Evaluation of placental function using near infrared spectroscopy during fetal growth restriction. J Perinat Med. 2010;38(1):29–32.
6. Kakogawa J, Kanayama N. Application of near-infrared spectroscopy for the evaluation of placental oxygenation. Open Med Devices J. 2012;4:22–7.
7. Sørensen A, Peters D, Simonsen C, Pedersen M, Stausbøl-Grøn B, Christiansen OB, et al. Changes in human fetal oxygenation during maternal hyperoxia as estimated by BOLD MRI. Prenat Diagn. 2013;33(2):141–5.
8. Sinding M, Peters DA, Frøkjær JB, Christiansen OB, Uldbjerg N, Sørensen A. Reduced placental oxygenation during subclinical uterine contractions as assessed by BOLD MRI. Placenta 2016;39:16–20.
9. Beard P. Biomedical photoacoustic imaging. Interface Focus. 2011;1(4):602–31.
10. Laufer J, Elwell C, Delpy D, Beard P. In vitro measurements of absolute blood oxygen saturation using pulsed near-infrared photoacoustic spectroscopy: accuracy and resolution. Phys Med Biol. 2005;50(18):4409.
11. Zhang HF, Maslov K, Sivaramakrishnan M, Stoica G, Wang LV. Imaging of hemoglobin oxygen saturation variations in single vessels in vivo using photoacoustic microscopy. Appl Phys Lett. 2007;90(5):053901.
12. Ishihara M, Shinchib M, Horiguchi A, Shinmotoc H, Tsudad H, Irisawae K et al, editors Possibility of transrectal photoacoustic imaging-guided biopsy for detection of prostate cancer. Proc of SPIE Vol; 2017.
13. Märk J, Wagener A, Pönick S, Grötzinger C, Zhang E, Laufer J, editors Motion corrected photoacoustic difference imaging of fluorescent contrast agents. SPIE BiOS; 2016: International Society for Optics and Photonics.
14. Petri M, Stoffels I, Jose J, Leyh J, Schulz A, Dissemond J, et al. Photoacoustic imaging of real-time oxygen changes in chronic leg ulcers after topical application of a haemoglobin spray: a pilot study. J Wound Care. 2016;25(2):87–91.
15. Petrov I, Petrov Y, Prough D, Cicenaite I, Deyo D, Esenaliev R. Optoacoustic monitoring of cerebral venous blood oxygenation though intact scalp in large animals. Opt Express. 2012;20(4):4159–67.
16. Needles A, Heinmiller A, Sun J, Theodoropoulos C, Bates D, Hirson D, et al. Development and initial application of a fully integrated photoacoustic micro-ultrasound system. IEEE Trans Ultrason Ferroelectr Freq Control. 2013;60(5):888–97.
17. Tzoumas S, Nunes A, Olefir I, Stangl S, Symvoulidis P, Glasl S, et al. Eigenspectra optoacoustic tomography achieves quantitative blood oxygenation imaging deep in tissues. arXiv preprint arXiv:151105846. 2015.
18. Sei K, Fujita M, Okawa S, Hirasawa T, Kushibiki T, Sasa H, et al. Appropriate timing of blood sampling for blood gas analysis in the ventilated rabbit. J Surg Res. 2016;206(2):325–36.
19. Song W, Wei Q, Liu W, Liu T, Yi J, Sheibani N, et al. A combined method to quantify the retinal metabolic rate of oxygen using photoacoustic ophthalmoscopy and optical coherence tomography. Sci Rep. 2014;4:6525.
20. Wang Y, Hu S, Maslov K, Zhang Y, Xia Y, Wang LV. In vivo integrated photoacoustic and confocal microscopy of hemoglobin oxygen saturation and oxygen partial pressure. Opt Lett. 2011;36(7):1029–31.
21. Prahl S. Optical absorption of hemoglobin, vol. 15. Oregon: Oregon Medical Laser Center; 1999. http://omlc.ogi.edu/spectra/hemoglobin/index.html.
22. Feiner JR, Rollins MD, Sall J, Eilers H, Au P, Bickler PE. Accuracy of carboxyhemoglobin detection by pulse CO-oximetry during hypoxemia. Anesth Analg. 2013;117(4):847.
23. Li W, Chen X. Gold nanoparticles for photoacoustic imaging. Nanomedicine 2015;10(2):299–320.
24. Beard P. Biomedical photoacoustic imaging. Interface Focus. 2011;2011:rsfs20110028.
25. Jiang Y, Forbrich A, Harrison T, Zemp RJ. Blood oxygen flux estimation with a combined photoacoustic and high-frequency ultrasound microscopy system: a phantom study. J Biomed Opt. 2012;17(3):0360121–8.
26. McGuill MW, Rowan AN. Biological effects of blood loss: implications for sampling volumes and techniques. ILAR J. 1989;31(4):5–20.
27. World Health Organization. Recommended methodology for using WHO international reference preparations for thromboplastin. Geneva: World Health Organization; 1983.
28. Vandegriff K, Olson J. The kinetics of O_2 release by human red blood cells in the presence of external sodium dithionite. J Biol Chem. 1984;259(20):12609–18.
29. Ishihara M, Sato M, Kaneshiro N, Mitani G, Sato S, Mochida J, et al. Development of a diagnostic system for osteoarthritis using a photoacoustic measurement method. Lasers Surg Med. 2006;38(3):249–55.
30. Fischer B, Chavatte-Palmer P, Viebahn C, Santos AN, Duranthon V. Rabbit as a reproductive model for human health. Reproduction 2012;144(1):1–10.
31. Lipman N, Marini R, Erdman S. A comparison of ketamine/xylazine and ketamine/xylazine/acepromazine anesthesia in the rabbit. Lab Anim Sci. 1990;40(4):395–8.
32. Lee RC. The rectal temperature of the normal rabbit. Am J Physiol Legacy Content. 1939;125(3):521–9.
33. Kim KS, Shim JC, Jun JH, Lee KH, Chung CW. Rabbits treated with chronic isepamicin are resistant to mivacurium and rocuronium. Anesth Analg. 1999;88(3):654–8.
34. Terakawa Y, Ichinohe T, Kaneko Y. Rocuronium and vecuronium do not affect mandibular bone marrow and masseter muscular blood flow in rabbits. J Oral Maxillofacial Surg. 2010;68(1):15–20.
35. Stahl WR. Scaling of respiratory variables in mammals. J Appl Physiol. 1967;22(3):453–60.
36. Drorbaugh JE. Pulmonary function in different animals. J Appl Physiol. 1960;15(6):1069–72.
37. Lowry DW, Mirakhur RK, McCarthy GJ, Carroll MT, McCourt KC. Neuromuscular effects of rocuronium during sevoflurane, isoflurane, and intravenous anesthesia. Anesth Analg. 1998;87(4):936–40.
38. Kiel J, Van Heuven W. Ocular perfusion pressure and choroidal blood flow in the rabbit. Investig Ophthalmol Vis Sci. 1995;36(3):579–85.
39. Aeschbacher G, Webb A. Propofol in rabbits. 2. Long-term anesthesia. Lab Anim Sci. 1993;43(4):328–35.
40. Shah PS, Shah VS. Continuous heparin infusion to prevent thrombosis and catheter occlusion in neonates with peripherally placed

percutaneous central venous catheters. Cochrane Library. 2008; CD002772.
41. Zotti A, Banzato T, Cozzi B. Cross-sectional anatomy of the rabbit neck and trunk: comparison of computed tomography and cadaver anatomy. Res Vet Sci. 2009;87(2):171–6.
42. Bland JM, Altman D. Statistical methods for assessing agreement between two methods of clinical measurement. Lancet 1986;327(8476):307–10.
43. Hanneman SK. Design, analysis and interpretation of method-comparison studies. AACN Adv Crit Care. 2008;19(2):223.
44. American National Standards Institute. Laser Institute of America, American National Standard for Safe Use of Lasers ANSI Z136.1-2014. New York: American National Standards Institute; 2014.
45. Mallidi S, Watanabe K, Timerman D, Schoenfeld D, Hasan T. Prediction of tumor recurrence and therapy monitoring using ultrasound-guided photoacoustic imaging. Theranostics 2015;5(3):289–301.
46. Lakshman M, Needles A. Screening and quantification of the tumor microenvironment with micro-ultrasound and photoacoustic imaging. Nat Methods. 2015;12(4):iii–v.
47. Esenaliev RO, Larina IV, Larin KV, Deyo DJ, Motamedi M, Prough DS. Optoacoustic technique for noninvasive monitoring of blood oxygenation: a feasibility study. Appl Opt. 2002;41(22):4722–31.
48. Laufer J, Delpy D, Elwell C, Beard P. Quantitative spatially resolved measurement of tissue chromophore concentrations using photoacoustic spectroscopy: application to the measurement of blood oxygenation and haemoglobin concentration. Phys Med Biol. 2006;52(1):141.
49. Hammer M, Schweitzer D, Michel B, Thamm E, Kolb A. Single scattering by red blood cells. Appl Opt. 1998;37(31):7410–8.
50. Sakota D, Takatani S. Photon-cell interactive Monte Carlo model based on the geometric optics theory for photon migration in blood by incorporating both extra-and intracellular pathways. J Biomed Opt. 2010;15(6):065001–14.
51. Kocsis L, Herman P, Eke A. The modified Beer–Lambert law revisited. Phys Med Biol. 2006;51(5):N91.
52. Friebel M, Do K, Hahn A, Mu G. Optical properties of circulating human blood in the wavelength range 400–2500 nm. J Biomed Opt. 1999;4(1):36–46.
53. Reynolds KJ, Palayiwa E, Moyle JT, Sykes MK, Hahn CE. The effect of dyshemoglobins on pulse oximetry: part I, theoretical approach and part II, experimental results using an in vitro test system. J Clin Monitor. 1993;9(2):81–90.
54. Verwaerde P, Malet C, Lagente M, De La Farge F, Braun J. The accuracy of the i-STAT portable analyser for measuring blood gases and pH in whole-blood samples from dogs. Res Vet Sci. 2002;73(1):71–5.
55. Zijlstra W, Buursma A, Meeuwsen-Van der Roest W. Absorption spectra of human fetal and adult oxyhemoglobin, de-oxyhemoglobin, carboxyhemoglobin, and methemoglobin. Clin Chem. 1991;37(9):1633–8.
56. Agusti A, Roca J, Barbera J, Casademont J, Rodriguez-Roisin R, Wagner P. Effect of sampling site on femoral venous blood gas values. J Appl Physiol. 1994;77(4):2018–22.
57. Ogoh S, Sato K, Okazaki K, Miyamoto T, Secher F, Sørensen H, et al. A decrease in spatially resolved near-infrared spectroscopy-determined frontal lobe tissue oxygenation by phenylephrine reflects reduced skin blood flow. Anesth Analg. 2014;118(4):823–9.